JOURNAL OF GEOPHYSICAL RESEARCH: PLANETS, VOL. 118, 1983–1990, doi:10.1002/jgre.20146, 2013

Simulations of the latitudinal variability of CO-like and OCS-like passive tracers below the clouds of Venus using the Laboratoire de Météorologie Dynamique GCM

E. Marcq[1,2] and S. Lebonnois[2]

Received 8 January 2013; revised 23 August 2013; accepted 28 August 2013; published 3 October 2013.

[1] The lower atmosphere of Venus below the clouds is a transitional region between the relatively calm lowermost scale height and the superrotating atmosphere in the cloud region and above. Any observational constraint is then welcome to help in the development of general circulation models of Venus, a difficult task considering the thickness of its atmosphere. Starting from a state-of-the-art 3-D Venus General Circulation Model (GCM), we have included passive tracers in order to investigate the latitudinal variability of two minor gaseous species, carbonyl sulfide (OCS) and carbon monoxide (CO), whose vertical profiles and mixing ratios are known to vary with latitude between 30 and 40 km. The relaxation to chemical equilibrium is crudely parametrized through a vertically uniform time scale τ. A satisfactory agreement with available observations is obtained with $10^8\text{s} \lesssim \tau_{\text{CO}} \lesssim 5 \cdot 10^8$ s and $10^7\text{s} \lesssim \tau_{\text{OCS}} \lesssim 10^8$ s. These results, in addition to validating the general circulation below the clouds, are also helpful in characterizing the chemical kinetics of Venus' atmosphere. This complements the much more sophisticated chemical models which focus more on thermodynamical equilibrium.

Citation: Marcq, E., and S. Lebonnois (2013), Simulations of the latitudinal variability of CO-like and OCS-like passive tracers below the clouds of Venus using the Laboratoire de Météorologie Dynamique GCM, *J. Geophys. Res. Planets*, *118*, 1983–1990, doi:10.1002/jgre.20146.

1. Introduction

[2] The near-infrared spectroscopy of Venus nightside has allowed to measure the composition of the deep atmosphere of Venus ever since the discovery of the so-called "infrared windows" [*Allen and Crawford*, 1984; *Crisp et al.*, 1989], spectral intervals in which the relatively weak opacity of CO_2 lets thermal radiation from the hot and dense troposphere of Venus escape through the cloud layers into space. In particular, the 1.74 μm window (probing H_2O and HCl around an altitude of 15 km) and the 2.3 μm window (probing CO, OCS, H_2O, HDO, HCl, HF, and SO_2 around an altitude of 30–40 km) have greatly expanded our knowledge of the lower Venusian atmospheric composition that was previously hindered by the overlying optically thick dense cloud layers.

[3] Numerous observations both from ground-based telescopes and from the *Venus Express* orbiter have yielded valuable observational constraints in the 2.3 μm window (see section 2 for more details). In particular, carbon monoxide (CO) and carbonyl sulfide (OCS) mixing ratios were found to exhibit vertical and/or latitudinal variability. This variability makes these minor species especially interesting in order to constrain modeling of both atmospheric chemistry and the deep general circulation since spectroscopic remote sensing retrieves abundances of minor species much more easily than measuring meridional and vertical winds.

[4] Such a strategy has been carried out successfully for Titan. Latitudinal contrasts of chemical compounds observed in the stratosphere by the *Voyager 1* spacecraft [*Coustenis and Bézard*, 1995] and the *Cassini* mission [*Flasar et al.*, 2005; *Coustenis et al.*, 2007] have been shown to result from the meridional circulation [*Lebonnois et al.*, 2001; *Hourdin et al.*, 2004; *Crespin et al.*, 2008]. These works used a general circulation model of Titan's atmosphere, coupled with transport of chemical compounds and full photochemistry or a simplified pseudochemistry based on relaxation toward given vertical profiles with chemically based time constants. The seasonal downwelling over the winter pole brings air from the high-altitude regions with high photochemical production of hydrocarbons and nitriles down into the polar stratosphere, which induces significant polar enrichment for most of these compounds at low-stratospheric altitudes.

[5] In the case of Venus, it is probable that the latitudinal variations observed for CO and OCS in the deep

[1]Laboratoire Atmosphères, Milieux, Observations Spatiales, Institut Pierre-Simon Laplace, CNRS UMR 8190, Université de Versailles Saint-Quentin-en-Yvelines, Guyancourt, France.
[2]Laboratoire de Météorologie Dynamique, Institut Pierre-Simon Laplace, CNRS UMR 8539, Université Paris 6, Paris, France.

Corresponding author: E. Marcq, LATMOS / IPSL / UVSQ, 11 Boulevard d'Alembert, F-78280 Guyancourt, France. (emmanuel.marcq@latmos.ipsl.fr)

2169-9097/13/10.1002/jgre.20146

Table 1. Mean Constraints on CO and OCS Vertical Profiles[a]

Species	Altitude (km)	Mixing Ratio q (ppm)	dq/dz (ppm/km)	Reference
CO	42	30 ± 18		*Oyama et al.* [1980]
	36	30 ± 7		*Gel'Man et al.* [1979]
	36	23 ± 5	1.2 ± 0.5	*Pollack et al.* [1993]
	35	26 ± 7	0.6 ± 0.5	*Taylor et al.* [1997]
	22	20 ± 3		*Oyama et al.* [1980]
	12	17 ± 5		*Gel'Man et al.* [1979]
OCS	38	0.35 ± 0.1		*Taylor et al.* [1997]
	33	4.4 ± 1	-1.58 ± 0.3	*Pollack et al.* [1993]
	30	14 ± 6		*Taylor et al.* [1997]

[a]Partially from *Krasnopolsky* [2007].

atmosphere are related to dynamical features. This hypothesis is tested in the study presented here. Using the three-dimensional general circulation model of Venus' atmosphere developed at the Laboratoire de Météorologie Dynamique (LMD-VGCM) [*Lebonnois et al.*, 2010], we have included semipassive tracers in order to explore the latitudinal variations produced by the atmospheric dynamics and compared them with observational constraints. The LMD-VGCM is briefly presented in section 3, as well as the methodology of our simulation experiments. The results of the simulations are detailed and discussed in section 4, and finally we summarize the implications of our findings in section 5.

[6] To some extent, our work can be considered as complementary to the work of *Yung et al.* [2009]. They built a 2-D chemical transport model to explain the observed CO and OCS distributions, using the wind field from an external 3-D-GCM [*Lee et al.*, 2007]. The meridional circulation of this GCM differs mainly from ours in its vertical structure. Our strategy here involves using a more sophisticated and up-to-date GCM [*Lebonnois et al.*, 2010], but a much simpler chemical parametrization. It will nevertheless be fruitful to compare the results of both studies.

2. Observational Constraints

[7] Measurements of CO and OCS under the clouds of Venus were first obtained by descent probes, but most of our knowledge comes from nightside spectroscopy in the 2.3 μm spectral window of CO_2 discovered by *Allen and Crawford* [1984]. Both ground-based observations and some spatial missions (*Galileo* flyby and, most importantly, the *Venus Express* orbiter) allowed a determination of the vertical profiles for altitudes ranging from 30 to 45 km of CO and OCS both in average and for specific locations. Recent reviews of observational constraints can be found in *Bézard and de Bergh* [2007] and *de Bergh et al.* [2006].

2.1. Mean Vertical Profiles

[8] In situ measurements by the *Pioneer Venus* probes and *Venera* landers [*Oyama et al.*, 1980; *Krasnopolsky and Parshev*, 1979; *Gel'Man et al.*, 1979] have constrained the mean mixing ratio of CO to the values mentioned in Table 1.

[9] About a decade afterward, spectroscopic studies [*Bézard et al.*, 1990; *Pollack et al.*, 1993; *Kamp et al.*, 1988] on the nightside in the 2.3 μm window could constrain the mean mixing ratio and vertical gradient of both CO and OCS profiles (see Table 1). These measurements are in a fairly good agreement with in situ measurements, although the vertical gradient derived by *Pollack et al.* [1993] was a little too steep to cope with *Pioneer Venus* measurements near 20 km. There is also a lack of consistency for the detection of OCS between *Pioneer Venus* and *Venera* measurements, but spectroscopic studies firmly derived a mean profile characterized by a very steep decrease [*Pollack et al.*, 1993] between 30 and 40 km.

[10] It is also worthy of note that various chemical models [*Krasnopolsky*, 2007; *Fegley and Treiman*, 1992; *Krasnopolsky and Pollack*, 1994] have successfully reproduced these values. Some model results appear in Table 1 along with observations.

2.2. Latitudinal Variability

[11] Once the mean profiles of both species were known, the focus shifted toward the determination of possible horizontal or temporal variations. Thus, using CO estimates based on retrievals from spectra collected by *NIMS/Galileo*, *Collard et al.* [1993] found that CO was more abundant ($35 \pm 15\%$) at higher northern latitudes (47°N) than near the equator. Ground-based studies using *SpeX/IRTF* at a higher spectral resolution [*Marcq et al.*, 2005, 2006] confirmed a similar enrichment in the southern hemisphere and found anticorrelated variations of OCS between 40°S and the equator. This anticorrelation was well reproduced by the 2-D dynamical-chemical model of *Yung et al.* [2009]. Some variations in the vertical gradients were also found for CO and OCS, steeper gradients being found at higher southern latitudes than at lower latitudes.

[12] More recent studies were performed using *VIRTIS/Venus Express* by *Marcq et al.* [2008] and *Tsang et al.* [2008]. These studies greatly extended the latitudinal coverage thanks to the quasi-polar orbit of *Venus Express*. The aforementioned trends for CO were confirmed up to 60° in both hemispheres, with a decrease of CO beyond this latitude seen by *VIRTIS-M* channel [*Tsang et al.*, 2008]. OCS measurements from *Marcq et al.* [2008] were mostly compatible with previous ground-based measurements.

[13] Finally, *AAT/IRIS2* high-resolution spectra were used by *Cotton et al.* [2012] in order to assess CO spatial and temporal variability. Their findings mostly confirm previously known trends (increase of CO abundance with increasing latitude between 0° and 60°), but in contrast with previous studies, most of the increase in CO takes place at altitudes around 45 ± 8 km (in all cases higher than 36 km). This is nevertheless compatible with the increase in the steepness of CO profile found by *Marcq et al.* [2006] with increasing latitudes. The summary of CO and OCS latitudinal variations are shown in Table 2.

Table 2. Latitudinal Variations of CO and OCS

Species	Latitude (deg)	Altitude (km)	Mixing ratio q (ppm)	dq/dz (ppm/km)	Reference
CO	80°S	36	~ 28		*Tsang et al.* [2008]
	60°S	36	31 ± 2		*Marcq et al.* [2008]
	60°S	35	32 ± 2		*Tsang et al.* [2008]
	40°S	35	28 ± 1.5		*Marcq et al.* [2005]
	30°S	36	26.5 ± 0.5	0.8 ± 0.2	*Marcq et al.* [2006]
	10°S	36	25.5 ± 0.5	0.4 ± 0.2	*Marcq et al.* [2006]
	10°S	36	25 ± 2		*Marcq et al.* [2008]
	0°	35	23 ± 2		*Tsang et al.* [2008]
	20°N	36	26 ± 1		*Marcq et al.* [2008]
	40°N	36	28 ± 2		*Marcq et al.* [2008]
	47°N	35	31 ± 4.5[a]		*Collard et al.* [1993]
	60°N	35	32 ± 2		*Tsang et al.* [2008]
	60°N	36	35 ± 5		*Marcq et al.* [2008]
	60°	40+	74 ± 10[b]		*Cotton et al.* [2012]
Species	Latitude (deg)	Altitude (km)	Mixing ratio q (ppm)	d ln q/d ln P	Reference
OCS	60°S	33	2.5 ± 1		*Marcq et al.* [2008]
	40°S	35	0.75 ± 0.25		*Marcq et al.* [2005]
	30°S	36	0.55 ± 0.1	5.5 ± 0.5	*Marcq et al.* [2006]
	10°S	36	0.55 ± 0.05	4.5 ± 0.5	*Marcq et al.* [2006]
	10°S	35	2 ± 0.5		*Marcq et al.* [2005]
	10°S	33	4 ± 1		*Marcq et al.* [2008]
	45°N	33	3 ± 1		*Marcq et al.* [2008]

[a]Assuming an equatorial mixing ratio of 23 ppm.
[b]Assuming a standard CO profile below 40 km and a uniform profile above.

3. The LMD Venus General Circulation Model

3.1. General Description

[14] The general circulation model used for our study has been under development at the LMD since 2005 [*Lebonnois et al.*, 2005, 2006, 2010]. We summarize some of its characteristics here and detail the introduction of pseudo-chemical tracers.

[15] Our model is a three-dimensional general circulation model, with a horizontal resolution of 48 longitudes by 32 latitudes, on 50 vertical levels (hybrid σ-levels/pressure levels grid) from the surface to roughly 100 km altitude. Topography is taken into account, using Magellan data smoothed to the GCM resolution. Solar forcing (including diurnal variations) is taken from tabulated fluxes [*Crisp*, 1986], and infrared radiation is computed using a Net Exchange Rates formulation developed specifically for the optically thick atmosphere of Venus [*Eymet et al.*, 2009]. Subgrid vertical turbulence (essentially the boundary layer), dry convective adjustment, and horizontal dissipation are parametrized, and a dumping of the winds is forced in the four topmost layers of the model (sponge layer). Compared to *Lebonnois et al.* [2010], the most noticeable change is the surface boundary layer scheme, which now includes a "Mellor and Yamada" parametrization [*Mellor and Yamada*, 1982], taken from the Earth version of the LMD-GCM and fully described in Appendix B of *Hourdin et al.* [2002]. This new boundary layer scheme improves significantly the temperature and wind profiles in the deep atmosphere between the surface and the cloud base. The simulation used for this work was started from rest and ran for 1000 Venusian days. Mean zonal wind field and mean meridional stream function are presented in Figure 1. Though the zonal winds are weaker than observed [*Schubert*, 1983; *Sánchez-Lavega et al.*, 2008], this modeled atmospheric structure is fairly consistent with observations.

[16] The tracer scheme introduced in the GCM allows to model a very simple linear chemistry, where chemical sources and sinks of a compound are represented by a relaxation of the mixing ratio toward a prescribed vertical profile. This profile is chosen to fit observations of this chemical compound. Once a steady state is reached, the distribution of a linearized chemical tracer results from a compromise between the advection by dynamics and relaxation to the prescribed profile.

[17] We have included in the GCM two kinds of tracers designed as "idealized" counterparts to the actual CO and OCS found in Venus' atmosphere. The choice of these

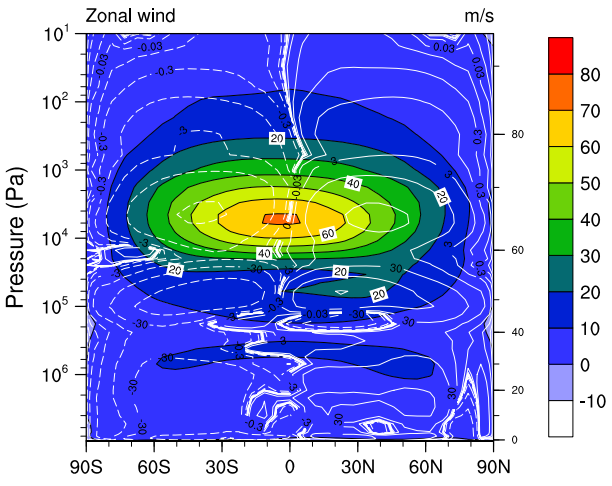

Figure 1. Mean zonal wind field (m s^{-1}) obtained in the GCM starting from rest after 1050 Venus days, averaged over longitudes and time. Contours indicate the mean stream function (unit is 10^9 kg s^{-1}), illustrating the averaged meridional circulation. The vertical coordinate on the right side of the plot stands for the geopotential height (in kilometers).

Table 3. Prescribed Profiles for CO and OCS

Species	Altitude (km)	q^0 (ppm)
CO	100	1000
	75	2
	64	50
	47	39
	22	20
	10	14
	0	14
OCS	64	0.005
	37	0.5
	30	20
	10	30
	0	30

species was straightforward since they are well constrained by the observations and their latitudinal variations clearly established as presented in section 2. The actual chemical balance between the sources and sinks for a given species indexed by i is modeled by a linear relaxation of its mole fraction $q_i(z, \varphi, \theta, t)$ toward a prescribed vertical profile ${q^0}_i(z)$, with a characteristic relaxation time τ_i. The net source term is then computed in the physical part of the model as

$$\left(\frac{\partial q_i(z,\varphi,\theta,t)}{\partial t}\right)_{\text{relaxation}} = \frac{{q^0}_i(z) - q_i(z,\varphi,\theta,t)}{\tau_i} \quad (1)$$

[18] This scheme is similar to the one already applied in the case of Titan for idealized tracers [*Lebonnois et al.*, 2001; *Hourdin et al.*, 2004].

3.2. Simulations

[19] We performed every simulation starting from the same initial state obtained after a reference run of 1000 Venusian days, without any tracers and starting from a resting state (Figure 1). This atmosphere exhibits a rather weak zonal wind field in the lower atmosphere compared to the observations. Tracers are then introduced and initialized according to their prescribed profile. Each simulation resumes then with the initialized tracer and run for 40 Venus days until a steady diurnal cycle for the tracer is reached or can be extrapolated if τ is too large (see subsection 3.2.2).

3.2.1. Relaxation Profiles

[20] Since the spectroscopic observations of the gaseous profiles yield $q(p)$ instead of $q(z)$—where p stands for the pressure—we have also adopted such a form for our relaxation profiles. More precisely, we set up several $q^0(p_k)$ at several pressure "control" levels p_k and interpolated $\ln[q^0(p)]$ linearly with respect to $\ln(p)$ between two control levels. This profiles' shape was adopted by most spectroscopy-based retrievals [*Pollack et al.*, 1993; *Marcq et al.*, 2005, 2006, 2008] and therefore enables a better comparison with observations.

[21] The mixing ratios of CO and OCS at the control levels can be found in Table 3 and come from standard references [*Bézard and de Bergh*, 2007; *Taylor et al.*, 1997; *Esposito et al.*, 1997]. Both profiles incidentally follow closely those derived from a thermochemical model found by *Krasnopolsky* [2007], indicating that the average vertical profiles of both species are already well understood by the available 1-D chemical models. Our preliminary tests had considered other profiles from spectroscopic studies [*Pollack et al.*, 1993], but these sources were reliable in the narrow altitude range probed by spectroscopy (30–40 km)—extrapolating mixing ratios at constant values above and under this range. The vertical mixing that occurs in the GCM requires a broader vertical coverage for the relaxation profile, at least between 15 and 55 km.

[22] It should also be noted that although the mean pressure and temperature profiles $p(z)$ and $T(z)$ within the model are quite similar to the standard VIRA-2 profiles [*Moroz and Zasova*, 1997], there is evidence for a large variability of these profiles in the atmosphere above 70 km [*Bertaux et al.*, 2007]. Some caution is therefore required when considering whether height or pressure is more suited to stand for the vertical dimension in the following discussions.

3.2.2. Extrapolation

[23] When the relaxation characteristic time τ is large (more than 10^8 s), the steady state cannot be achieved even after 40 simulated Venusian days. Fortunately, the temporal evolution of $\bar{q}_i(z,t)$ (where $\bar{q}_i$ stands for the longitudinal average on the nightside hemisphere) is empirically found to follow an exponentially asymptotic behavior : $\bar{q}_i(t) \rightarrow Q_i + A_i \cdot \exp(-B_i \cdot t)$ for large enough values of t (typically discarding the first values of $\bar{q}_i(t)$ for $t < \tau_i/4$) as can be seen in Figure 2. Using a standard least squares Levenberg-Marquardt fit, it is possible to retrieve A_i, B_i, and Q_i. We therefore consider that the asymptotic value Q_i is a good approximation for the tracer's steady state value, thus removing the need for impractically long simulations.

[24] It is mildly surprising that such a simple extrapolation is in a good agreement with the actual evolution of the synthetic tracers in the GCM for such a complex, multivariate nonlinear dynamical system in a chaotic state such as Venus' atmosphere. Even when considering a linearized subsystem such as our prescribed synthetic tracers, one would expect a superposition of several exponents with a number of time scales, and our fitting procedure would only catch

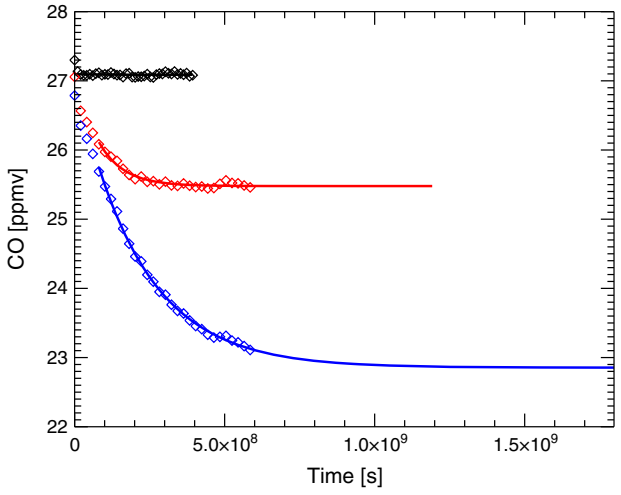

Figure 2. Evolution of CO-like simulated tracers at a pressure level of 5.53 bar (35 km) near the equator for various relaxation time scales (black: 10^7 s, red: 10^8 s, blue: $3 \cdot 10^8$ s). Diamonds show the GCM-computed values, whereas the solid lines stand for the best fit exponential extrapolations toward asymptotic values. The agreement is very satisfying and shows that the asymptotic value is reached for $\tau_i < 2 \cdot 10^8$ s and can be extrapolated safely for $\tau_i < 10^9$ s.

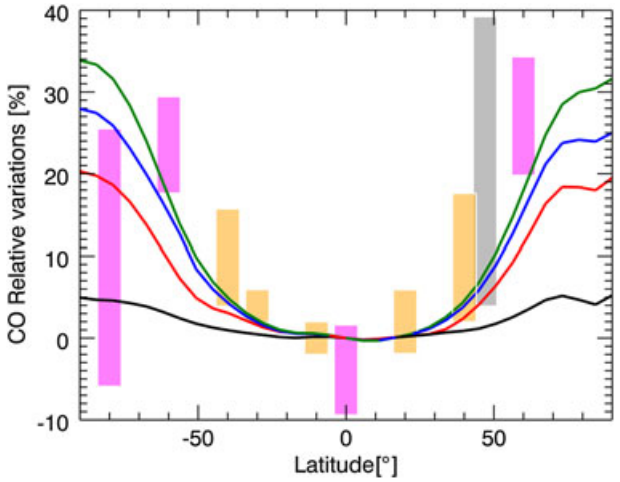

Figure 3. Relative latitudinal variations of the zonal average of synthetic CO-like tracers at $P = 5.5$ bar and comparison with observations. Solid lines stand for various relaxation time scales (black: 10^7 s, red: 10^8 s, blue: $3 \cdot 10^8$ s, green: $5 \cdot 10^8$ s). Colored bars stand for observational constraints (orange: SpeX/IRTF, pink: VIRTIS/*Venus Express*, gray: NIMS/*Galileo*).

the shortest one. However, Figure 2 demonstrates that (1) for $\tau_i < 10^8$s, the steady state reached by our simulation does not differ significantly from our extrapolation, so that the extrapolation can be dispensed with without altering our conclusions and (2) the agreement for shorter time scales gives us confidence that, at least for τ_i in the 10^8 to 10^9 s range, the extrapolation will be reasonably close to the not yet reached steady state. However, our fitting method only works if $q_i(t)$ is seen to vary over the simulation; therefore, the total simulation time has to be comparable to τ_i, which precludes a study for τ_i larger than about 10^9s.

4. Results

4.1. Carbon Monoxide

[25] Meaningful comparison between latitudinal variability of the simulated tracers and observations requires a careful choice of the relevant observable parameter. We have chosen to examine CO variability at a (fixed) pressure level of 5.5 bar (corresponding to a VIRA-2 altitude of about 36 km), matching the peak sensitivity of the 2.3 μm spectroscopic measurements. It is also worth noting that spectroscopic observations have a greater accuracy in measuring variations of CO than in measuring absolute values of the CO mixing ratio, since the main source of uncertainty in the modeling of the CO (2-0) band lies in the poorly known CO_2-CO_2 continuum opacity and not in variable factors such as the overlying scattering clouds. Therefore, it is more useful to study the relative variations of CO with respect to, e.g., the equatorial value rather than actual mixing ratios. Results are shown in Figure 3 for various relaxation times.

[26] First it appears that the actual magnitude of these variations is well reproduced by our synthetic tracers provided the relaxation time is on the order of 10^8 s at least. This behavior is easily understood: a faster relaxation to the prescribed profile hinders any variability induced by the circulation. Also, since CO mixing ratio is increasing with increasing altitude, the comparatively higher mixing ratios at higher latitudes are indicative of ascending circulation at lower latitudes and/or subsidence at higher latitudes, typical of a symmetric, Hadley-cell-like circulation. Such long relaxation time scales compared with the zonal superrotation also preclude any significant zonal variability.

[27] However, the quantitative comparison between synthetic tracers and observations shows that the enrichment with increasing latitude takes place at higher latitudes for the synthetic tracers. Whereas CO mixing ratio peaks near 60° in both hemispheres according to observations, this maximum is reached only between 70° and 80° in our modeling. The suspected decrease past 60° is also absent in our simulations or at the very least quite minor. In general, also, the latitudinal gradient seems too steep past 50° and not steep enough at lower latitudes. The magnitude of the variations seems a little too large for $\tau = 5 \cdot 10^8$ s, but we could not test larger time scales within a reasonable computing time. Therefore, we are only able to estimate the lower bound of this relaxation time from these observations. Let us finally note that none of our models naturally reproduces a much stronger variability at higher altitudes as observed by *Cotton et al.* [2012], but it may be due to our vertically uniform relaxation time, whose extrapolation may be invalid above 40 km. However, it is hard to prescribe even longer relaxation times to allow for a larger variability above 40 km since the optimal uniform value for τ is already very long and longer relaxation times are unable to increase latitudinal variability (Figure 3).

[28] Other constraints can in principle be derived by comparing the vertical gradient of the tracers at fixed latitudes with the one observed for CO around 36 km. Such a comparison is shown in Figure 4. We first notice that, as could be expected, the longer the relaxation time, the smoother the profiles are. Second, the average vertical gradients all lie reasonably within the observational constraints. But,

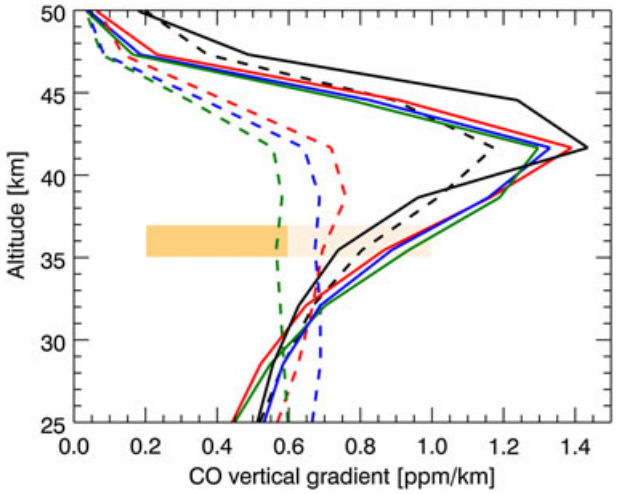

Figure 4. Vertical profile of the zonal average of the *vertical gradient* of synthetic CO-like tracers at latitudes of 0° (solid lines) and 67.5°N (dashed lines). The color code is the same as in Figure 3. Yellow boxes stand for observational constraints from *Marcq et al.* [2006] at 10°S (dark orange) and 30°S (light orange).

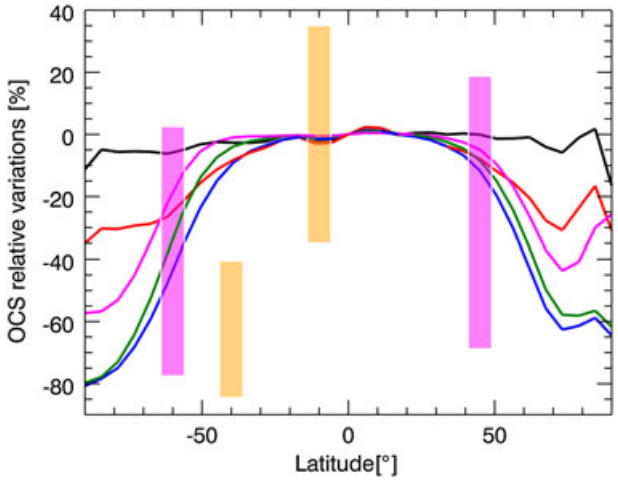

Figure 5. Relative latitudinal variations of the zonal average of synthetic OCS-like tracers at $P = 7.7$ bar and comparison with observations. Solid lines stand for various relaxation time scales (black: 10^6 s, red: 10^7 s, blue: 10^8 s, green: $3 \cdot 10^8$ s, magenta: $5 \cdot 10^8$ s). Colored bars stand for observational constraints (orange: SpeX/IRTF, pink: VIRTIS/*Venus Express*).

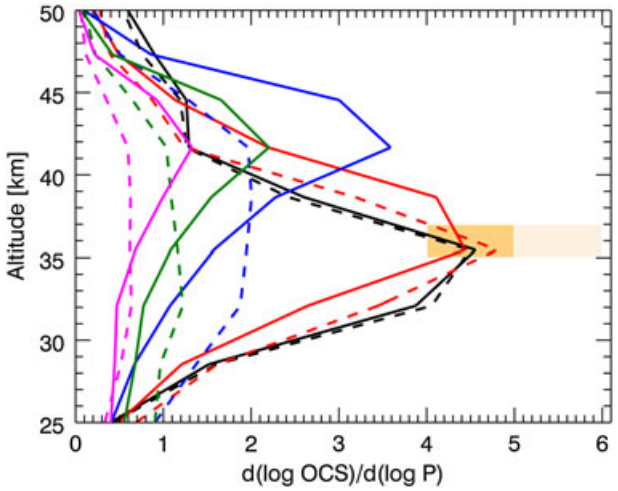

Figure 7. Vertical profile of the zonal average of the *vertical logarithmic gradient* of synthetic OCS-like tracers at latitudes of 0° (solid lines) and 67.5°N (dashed). The color code is the same as in Figure 5. Yellow boxes stand for observational constraints from *Marcq et al.* [2006] at 10°S (dark orange) and 30°S (light orange).

whereas steeper profiles with increasing latitude were observed, the opposite trend is found for the synthetic tracers. This is probably linked to our prescribing a vertically uniform relaxation time for each synthetic tracer, which is probably too simplistic an assumption. Or it could point out that the details of the vertical circulation below the clouds, quite weak compared to the cloud region and above, are not accurately computed in the GCM. In all cases, the profiles at higher latitudes computed for time scales longer than $5 \cdot 10^8$ s seem not steep enough compared to observational constraints, so it can help us in narrowing down the acceptable range for the vertically averaged relaxation time for CO near an altitude of 36 km: between 10^8 and $5 \cdot 10^8$ s. Let us keep in mind that the assumptions we have made only allow to determine the order of magnitude of the chemical relaxation time constant. It is, however, noteworthy that this is comparable to the mean Lagrangian time scale, suggesting a mostly dynamic control of CO variability in this altitude range.

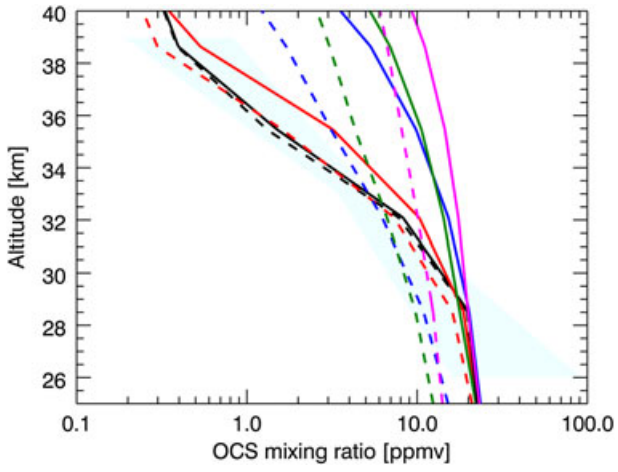

Figure 6. Vertical profile of the zonal average of OCS-like tracers at latitudes of 0° (solid) and 67.5°N (dashed). The color code is the same as in Figure 5. The cyan polygon stands for observational constraints from *Pollack et al.* [1993].

4.2. Carbonyl Sulfide

[29] Carbonyl sulfide variations with latitude are far less well constrained by observations than those of carbon monoxide. Our model shows (see Figure 5, centered on $P = 7.7$ bar, equivalent to a VIRA-2 altitude of about 32 km) that a negative gradient with increasing latitude is expected, with larger variations associated with longer time scales. The decreasing vertical gradient for OCS means that the qualitative explanation that we proposed for CO is confirmed: any vertical advection will simultaneously affect CO and OCS mixing ratios in opposite ways. Unfortunately, observational constraints on the latitudinal variability only are too lax to help us to determine precisely the relaxation time scale of our synthetic tracers. At most, we can state that time scales shorter than 10^7 s appear too short to enable any significant latitudinal variability, which is not impossible but quite unlikely.

[30] Fortunately, OCS mean vertical profile in the 30–40 km altitude range exhibits a very steep, dramatic decrease by a factor of 100. This behavior is hard for chemical models to reproduce successfully [*Yung et al.*, 2009], but observations in the 2.3 μm window require such a steep vertical gradient. *Pollack et al.* [1993] were the first to properly fit the observations using a constant logarithmic gradient $\frac{\mathrm{d}\log(q_{\mathrm{OCS}})}{\mathrm{d}\log P}$ in the 26–39 km range, and the relative uncertainty on this slope is far less than for latitudinal variations. Comparisons with observations are shown in Figures 6 and 7. It appears from these figures that only quite short time scales ($< 10^8$ s) are able to maintain a realistically steep enough vertical gradient. We can therefore narrow the most likely

range for OCS chemical relaxation between 10^7 s (to allow for some latitudinal variability) and 10^8 s (to ensure a steep enough vertical gradient).

5. Discussion and Conclusion

[31] First of all, it appears that the qualitative agreement between the ideal synthetic tracers and their observed counterparts is satisfying. This provides an a posteriori legitimation for our basic assumptions, namely,

[32] 1. that the latitudinal variability of CO and OCS in the lower atmosphere of Venus is caused by competing effects of global-scale dynamics, enhancing these contrasts, and chemical reactions acting locally toward restoring equilibrium abundances, thus suppressing these contrasts;

[33] 2. and that these departures from chemical equilibrium are small enough to be linearized, with constant time scales in the altitude range where observations are available (namely, between 30 and 40 km).

[34] Quantitative agreement is also reached for some crucial observable parameters (magnitude of CO latitudinal variations, OCS vertical steepness for the observed profile) but not for all of them, far from it. It is too soon to tell whether this comes from shortcomings in the dynamics of the GCM—the 30–40 km region is not the main focus during the testing of the GCM since we have very few dynamical observations—or, more probably, whether this comes from an oversimplified chemical scheme. A possible improvement would be to prescribe variable relaxation time $\tau(z)$ vertical profiles, but we preferred for this study to keep tunable ad hoc parameters to as few as possible. The relaxation profile themselves could also be altered a little to accommodate observations better, although we expect it would result only in marginal improvements of the quantitative agreement, resulting in a modest shift of the optimal τ values.

[35] An interesting consequence of our study is that typical relaxation times for CO and OCS seem to differ by at least 1 order of magnitude. This at least implies that the rate-determining step in the processes involving CO and OCS is not the same for CO and for OCS.

[36] CO mixing ratio is more probably controlled by the steady flux coming from the upper atmosphere. Its relaxation time scale ($\tau_{CO} \sim 1 - 5 \cdot 10^8$ s) is actually very close to the typical transport time scale along the Hadley cell (between 10^8 and 10^9 s), so that CO is actually behaving like a passive tracer in the 30–40 altitude range. Further support for this claim comes from the time scale of the fastest reaction involving CO according to *Krasnopolsky* [2007] in the same altitude range (which acts as a sink for CO): $SO_3 + CO \rightarrow CO_2 + SO_2$. Its reaction rate is $\nu' \sim 2 \cdot 10^5 \mathrm{cm}^{-3}\,\mathrm{s}^{-1}$, which yields a corresponding characteristic lifetime of about $2 \cdot 10^{10}$ s. This value lies 2 orders of magnitude above our upper limit for τ_{CO} and of the transport time scale, which in other words means that it is inefficient in governing the CO meridional distribution.

[37] On the other hand, OCS mixing ratio is more probably controlled by chemistry rather than dynamics ($\tau_{OCS} \sim 10^7 - 10^8$ s). This also appears to be in quantitative agreement with recent chemical modeling [*Krasnopolsky*, 2007]: according to their study, the main sink for OCS above 35 km is the reaction $OCS + SO_3 \rightarrow CO_2 + (SO)_2$ with a reaction rate $\nu \sim 5 \cdot 10^6\ \mathrm{cm}^{-3}\,\mathrm{s}^{-1}$. This translates to a typical lifetime $\tau = q_{OCS}/\nu \sim 3 \cdot 10^7$ s, which is in perfect agreement with the interval we derived for OCS. We are then able to confirm not only that this reaction probably controls the mean vertical profile of OCS above 30 km but also that its competition with dynamics is in control of its latitudinal variability. However, this reaction has no laboratory basis and its reaction rate is purely hypothesized in *Krasnopolsky* [2007]. *Yung et al.* [2009] proposed other possible sink chemical paths for OCS: photosensitized dissociation of OCS via the photochemistry of S_x resulting in $OCS + S \rightarrow CO + S_2$ or some unknown heteregenous reactions taking place within the lower haze below the clouds.

[38] As for the comparison with *Yung et al.* [2009], there is an interesting qualitative agreement in the reaction rate of their postulated OCS sink (about $10^{-8}\ \mathrm{s}^{-1}$) and our OCS lifetime, with a missing factor 3 that can be ascribed to the differences between the circulations in the different GCM used. The more satisfying agreement with *Krasnopolsky* [2007] brings more credence to the identification of the OCS sink with the destruction initiated by SO_3 originating from the evaporation and thermal dissociation of the overlying H_2SO_4 clouds, which was a candidate reaction also suggested by *Yung et al.* [2009]. They also suggest, from the fact that $q_{CO} + q_{OCS}$ is constant with latitude within observational error, that the sink for OCS also acts as a source for CO. The order-of-magnitude difference we find for the lifetimes of CO and OCS, as well as our probable identification of the OCS sink reaction, implies that their conclusion can only be valid for the net chemical balance but that no elementary process is directly converting OCS to CO.

[39] The results presented in this work are certainly sensitive to the details of the modeled circulation. Alterations in the angular momentum budget (through different settings and/or additional parameterizations) would affect the distribution of zonal wind and its vertical profile in the lower cloud region and below. However, the vertical organization of the meridional circulation is mainly driven by the vertical structure of the thermal forcing and is quite robust to the details of the GCM settings. As an illustration, we are currently working on new simulations that include a tentative new parameterization for gravity waves (based on a parameterization developed for the Earth by *Lott et al.* [2012]) and that are started from an atmosphere already in superrotation. Though these simulations are not finalized and are not yet suitable for publication, the introduction of this additional process affects the angular momentum budget and modifies both the amplitude of the peak zonal wind and its vertical gradient in the lower clouds and below. In these new conditions, the associated meridional circulation is fairly similar as the one shown in this work, both in structure and amplitude (within a factor of roughly 2). When including the same tracers, results are similar and yield similar conclusions, which illustrates the robustness of our results to the details of the global circulation. Thus, the orders of magnitude for CO and OCS time scales seem robust with respect to the details of the dynamics, provided large-scale Hadley-like circulation exists in these simulations in order to create the latitudinal variability in the first place.

[40] In all cases, the success of our modeling brings evidence that the LMD-GCM of Venus is now mature enough so that more realistic, full-scale kinetic chemical submodels may be safely embedded in order to further increase our

understanding of the interplay between dynamics and chemistry in Venus' atmosphere—although simplified chemical modeling comparable to ours could still give interesting insights even for the upper part of the atmosphere where minor species such as SO_2 experience spatial and temporal variability on a wide range of time scales [*Encrenaz et al.*, 2012; *Marcq et al.*, 2013].

[41] **Acknowledgments.** We wish to thank the ANR for its financial support to the "Exoclimats" project in which this study was planned. We also wish to acknowledge support from the CNES who funded E. Marcq's postdoctoral research grant on this topic.

References

Allen, D. A., and J. W. Crawford (1984), Cloud structure on the dark side of Venus, *Nature*, *307*, 222–224.

Bertaux, J.-L., et al. (2007), A warm layer in Venus' cryosphere and high-altitude measurements of HF, HCl, H_2O and HDO, *Nature*, *450*, 646–649, doi:10.1038/nature05974.

Bézard, B., and C. de Bergh (2007), Composition of the atmosphere of Venus below the clouds, *J. Geophys. Res.*, *112*, E04S07, doi:10.1029/2006JE002794.

Bézard, B., C. de Bergh, D. Crisp, and J.-P. Maillard (1990), The deep atmosphere of Venus revealed by high-resolution nightside spectra, *Nature*, *345*, 508–511, doi:10.1038/345508a0.

Collard, A. D., et al. (1993), Latitudinal distribution of carbon monoxide in the deep atmosphere of Venus, *Planet. Space Sci.*, *41*, 487–494, doi:10.1016/0032-0633(93)90033-X.

Cotton, D. V., J. Bailey, D. Crisp, and V. S. Meadows (2012), The distribution of carbon monoxide in the lower atmosphere of Venus, *Icarus*, *217*, 570–584, doi:10.1016/j.icarus.2011.05.020.

Coustenis, A., and B. Bézard (1995), Titan's atmosphere from Voyager infrared observations. 4: Latitudinal variations of temperature and composition, *Icarus*, *115*, 126–140, doi:10.1006/icar.1995.1084.

Coustenis, A., et al. (2007), The composition of Titan's stratosphere from Cassini/CIRS mid-infrared spectra, *Icarus*, *189*, 35–62, doi:10.1016/j.icarus.2006.12.022.

Crespin, A., S. Lebonnois, S. Vinatier, B. Bézard, A. Coustenis, N. A. Teanby, R. K. Achterberg, P. Rannou, and F. Hourdin (2008), Diagnostics of Titan's stratospheric dynamics using Cassini/CIRS data and the 2-dimensional IPSL circulation model, *Icarus*, *197*, 556–571, doi:10.1016/j.icarus.2008.05.010.

Crisp, D. (1986), Radiative forcing of the Venus mesosphere. I—Solar fluxes and heating rates, *Icarus*, *67*, 484–514, doi:10.1016/0019-1035(86)90126-0.

Crisp, D., W. M. Sinton, K.-W. Hodapp, B. Ragent, F. Gerbault, and J. H. Goebel (1989), The nature of the near-infrared features on the Venus night side, *Science*, *246*, 506–509.

de Bergh, C., V. I. Moroz, F. W. Taylor, D. Crisp, B. Bézard, and L. V. Zasova (2006), The composition of the atmosphere of Venus below 100 km altitude: An overview, *Planet. Space Sci.*, *54*, 1389–1397, doi:10.1016/j.pss.2006.04.020.

Encrenaz, T., T. K. Greathouse, H. Roe, M. Richter, J. Lacy, B. Bézard, T. Fouchet, and T. Widemann (2012), HDO and SO_2 thermal mapping on Venus: Evidence for strong SO_2 variability, *Astron. Astrophys.*, *543*, A153, doi:10.1051/0004-6361/201219419.

Esposito, L. W., J.-L. Bertaux, V. Krasnopolsky, V. I. Moroz, and L. V. Zasova (1997), Chemistry of lower atmosphere and clouds, in *Venus II: Geology, Geophysics, Atmosphere, and Solar Wind Environment*, edited by S. W. Bougher et al., p. 415, University of Arizona Press, Tucson, AZ.

Eymet, V., R. Fournier, J.-L. Dufresne, S. Lebonnois, F. Hourdin, and M. A. Bullock (2009), Net exchange parameterization of thermal infrared radiative transfer in Venus' atmosphere, *J. Geophys. Res.*, *114*, E11008, doi:10.1029/2008JE003276.

Fegley, B., and A. Treiman (1992), Chemistry of the surface and lower atmosphere of Venus, *Astron. Vestn.*, *26*, 3–65.

Flasar, F. M., et al. (2005), Titan's atmospheric temperatures, winds, and composition, *Science*, *308*, 975–978, doi:10.1126/science.1111150.

Gel'Man, B. G., V. G. Zolotukhin, N. I. Lamonov, B. V. Levchuk, A. N. Lipatov, L. M. Mukhin, D. F. Nenarokov, V. A. Rotin, and B. P. Okhotnikov (1979), Analysis of chemical composition of Venus atmosphere by gas chromatography on Venera 12, *Cosmic Res.*, *17*, 585–589.

Hourdin, F., F. Couvreux, and L. Menut (2002), Parameterization of the dry convective boundary layer based on a mass flux representation of thermals, *J. Atmos. Sci.*, *59*, 1105–1123, doi:10.1175/1520-0469(2002)059<1105:POTDCB>2.0.CO;2.

Hourdin, F., S. Lebonnois, D. Luz, and P. Rannou (2004), Titan's stratospheric composition driven by condensation and dynamics, *J. Geophys. Res.*, *109*, E12005, doi:10.1029/2004JE002282.

Kamp, L. W., F. W. Taylor, and S. B. Calcutt (1988), Structure of Venus's atmosphere from modelling of night-side infrared spectra, *Nature*, *336*, 360–362, doi:10.1038/336360a0.

Krasnopolsky, V. A. (2007), Chemical kinetic model for the lower atmosphere of Venus, *Icarus*, *191*, 25–37, doi:10.1016/j.icarus.2007.04.028.

Krasnopolsky, V. A., and V. A. Parshev (1979), Chemical composition of the Venusian troposphere and cloud layer from measurements of Venera 11 and 12 and Pioneer-Venus, *Cosmol. Res.*, *17*, 763–771.

Krasnopolsky, V. A., and J. B. Pollack (1994), H_2O-H_2SO_4 system in Venus' clouds and OCS, CO, and H_2SO_4 profiles in Venus' troposphere, *Icarus*, *109*, 58–78, doi:10.1006/icar.1994.1077.

Lebonnois, S., D. Toublanc, F. Hourdin, and P. Rannou (2001), Seasonal variations of Titan's atmospheric composition, *Icarus*, *152*, 384–406, doi:10.1006/icar.2001.6632.

Lebonnois, S., F. Hourdin, V. Eymet, R. Fournier, and J.-L. Dufresne (2005), A new Venus General Circulation Model, in the context of the Venus-Express mission, *Bull. Am. Astron. Soc.*, *37*, 742.

Lebonnois, S., A. Crespin, F. Hourdin, V. Eymet, R. Fournier, and J.-L. Dufresne (2006), Super-rotation simulated with the new LMD Venus General Circulation Model, *European Planetary Science Congress 2006,* pp. 167, Berlin, Germany.

Lebonnois, S., F. Hourdin, V. Eymet, A. Crespin, R. Fournier, and F. Forget (2010), Superrotation of Venus' atmosphere analyzed with a full general circulation model, *J. Geophys. Res.*, *115*, E06006, doi:10.1029/2009JE003458.

Lee, C., S. R. Lewis, and P. L. Read (2007), Superrotation in a Venus General Circulation Model, *J. Geophys. Res.*, *112*, E04S11, doi:10.1029/2006JE002874.

Lott, F., L. Guez, and P. Maury (2012), A stochastic parameterization of non-orographic gravity waves: Formalism and impact on the equatorial stratosphere, *Geophys. Res. Lett.*, *39*, L06807, doi:10.1029/2012GL051001.

Marcq, E., B. Bézard, T. Encrenaz, and M. Birlan (2005), Latitudinal variations of CO and OCS in the lower atmosphere of Venus from near-infrared nightside spectro-imaging, *Icarus*, *179*, 375–386, doi:10.1016/j.icarus.2005.06.018.

Marcq, E., T. Encrenaz, B. Bézard, and M. Birlan (2006), Remote sensing of Venus' lower atmosphere from ground-based IR spectroscopy: Latitudinal and vertical distribution of minor species, *Planet. Space Sci.*, *54*, 1360–1370, doi:10.1016/j.pss.2006.04.024.

Marcq, E., B. Bézard, P. Drossart, G. Piccioni, J. M. Reess, and F. Henry (2008), A latitudinal survey of CO, OCS, H_2O, and SO_2 in the lower atmosphere of Venus: Spectroscopic studies using VIRTIS-H, *J. Geophys. Res.*, *113*, E00B07, doi:10.1029/2008JE003074.

Marcq, E., J.-L. Bertaux, F. Montmessin, and D. Belyaev (2013), Variations of sulphur dioxide at the cloud top of Venus's dynamic atmosphere, *Nat. Geosci.*, *6*(1), 25–28, doi:10.1038/ngeo1650.

Mellor, G. L., and T. Yamada (1982), Development of a turbulence closure model for geophysical fluid problems, *Rev. Geophys. Space Phys.*, *20*, 851–875, doi:10.1029/RG020i004p00851.

Moroz, V. I., and L. V. Zasova (1997), VIRA-2: A review of inputs for updating the Venus International Reference Atmosphere, *Adv. Space Res.*, *19*, 1191–1201.

Oyama, V. I., G. C. Carle, F. Woeller, J. B. Pollack, R. T. Reynolds, and R. A. Craig (1980), Pioneer Venus gas chromatography of the lower atmosphere of Venus, *J. Geophys. Res.*, *85*, 7891–7902.

Pollack, J. B., et al. (1993), Near-infrared light from Venus' nightside—A spectroscopic analysis, *Icarus*, *103*, 1–42, doi:10.1006/icar.1993.1055.

Sánchez-Lavega, A., et al. (2008), Variable winds on Venus mapped in three dimensions, *Geophys. Res. Lett.*, *35*, L13204, doi:10.1029/2008GL033817.

Schubert, G. (1983), General circulation and the dynamical state of the Venus atmosphere, in *Venus (A83-37401 17-91)*, edited by S. W. Bougher, D. M. Hunten, and R. J. Phillips, pp. 681–765, University of Arizona Press, Tucson, AZ.

Taylor, F. W., D. Crisp, and B. Bézard (1997), Near-infrared sounding of the lower atmosphere of Venus, in *Venus II*, edited by D. M. Hunten et al., pp. 325–351, University of Arizona Press, Tucson.

Tsang, C. C. C., P. G. J. Irwin, C. F. Wilson, F. W. Taylor, C. Lee, R. de Kok, P. Drossart, G. Piccioni, B. Bézard, and S. Calcutt (2008), Tropospheric carbon monoxide concentrations and variability on Venus from Venus Express/VIRTIS-M observations, *J. Geophys. Res.*, *113*, E00B08, doi:10.1029/2008JE003089.

Yung, Y. L., M. C. Liang, X. Jiang, R. L. Shia, C. Lee, B. Bézard, and E. Marcq (2009), Evidence for carbonyl sulfide (OCS) conversion to CO in the lower atmosphere of Venus, *J. Geophys. Res.*, *114*, E00B34, doi:10.1029/2008JE003094.